Soft Matter

RSC Publishing

PAPER

View Article Online
View Journal | View Issue

Cite this: *Soft Matter*, 2013, **9**, 758

Decoding membrane- *versus* receptor-mediated delivery of single-walled carbon nanotubes into macrophages using modifications of nanotube surface coatings and cell activity†

Patrick D. Boyer,[a] Brian D. Holt,[b] Mohammad F. Islam*[c] and Kris Noel Dahl*[ab]

Therapeutic applications of single-walled carbon nanotubes (SWCNTs) require understanding uptake mechanisms in macrophages, which are involved with many physiological and pathological processes. However, therapeutic applications are limited by poor quantification and mechanistic understanding of uptake into macrophages with different levels of activation. We find delivery of more than 50 million SWCNTs per cell to activated macrophages, which is 10× more than unactivated macrophages and 100× more than fibroblasts. Determining the mechanisms of SWCNT uptake is important for tuning this specific delivery, but standard cellular assays are inapplicable with SWCNTs, which quench fluorescence. By modification of surface coatings on the SWCNTs and altering macrophage activation, we applied models of macrophage uptake of SWCNTs and quantified precise model parameters. With this model, we show receptor-mediated processes saturate, and above the saturation levels we observe little added delivery as well as a reduction in cell proliferation and visibly altered cell morphology. Thus, SWCNTs can be preferentially delivered to activated macrophages, and the model of uptake suggests delivery is optimized between high extracellular levels and receptor saturation.

Received 28th August 2012
Accepted 23rd October 2012

DOI: 10.1039/c2sm26995c

www.rsc.org/softmatter

Introduction

Understanding the interactions between nanomaterials and immune cells and quantifying uptake precisely are important both for determining toxicity and for developing medical therapeutics related to cancer, inflammation, wound healing and regenerative medicine. Macrophages from monocytes and resident tissue macrophages are responsible for removing unwanted materials and cellular debris from the body, particularly in the M1 or pro-inflammatory phenotype.[1] These cells would likely be the first to encounter therapeutic materials[2] and thus are largely responsible for dictating the fate, processing and ultimate effect of those materials. Local macrophage concentration increases in regions of infection, inflammation and wound healing, as well as in pathological regions including tumor environments and regions of atherosclerosis.[3,4] Targeted delivery of nanomaterials to macrophages could potentially be utilized for more precise imaging of macrophages within the body, as well as drug delivery and thermal ablation of macrophages.[5] Additionally, macrophages loaded with nanomaterials offer the exciting potential of cell-mediated drug delivery as these cells can cross the blood–brain barrier.[6]

Recent studies have shown the potential for single-walled carbon nanotubes (SWCNTs) as drug and gene delivery vectors,[7] imaging probes for cellular labeling,[8,9] tracking agents[10–12] and molecular sensors.[13,14] SWCNTs are hydrophobic materials that aggregate in water leading to diminished optical properties[15] and deleterious cellular effects.[16] SWCNTs have been dispersed through various covalent modifications and noncovalent functionalization with poly(ethylene oxide) (PEO) based copolymers,[8,17] lipids,[5,18] DNA,[19] peptides,[20] and proteins.[21–25] Well-dispersed individual SWCNTs have been used in cellular applications without acute toxicity.[17]

Cellular uptake of and response to SWCNTs are also impacted by SWCNT functionalization and cell type. In direct comparisons, macrophages show increased nanoparticle uptake efficiency over epithelial, astrocytes and endothelial cell types.[26] For targeting to macrophages, it is unclear if nanomaterial surface coating or cell activation state is the dominant factor for cell uptake. Macrophages treated with lipopolysaccharide (LPS) to produce an M1 phenotype[1] show altered immune response after treatment with functionalized nanomaterials.[27] Conversely, some functionalized SWCNTs provoke

[a]*Department of Chemical Engineering, Carnegie Mellon University, Pittsburgh, PA, USA*

[b]*Department of Biomedical Engineering, Carnegie Mellon University, Pittsburgh, PA, USA. E-mail: krisdahl@cmu.edu*

[c]*Department of Material Science and Engineering, Carnegie Mellon University, Pittsburgh, PA, USA. E-mail: mohammad@cmu.edu*

† Electronic supplementary information (ESI) available: Derivation of cell uptake model, localization of SWCNTs in macrophages, fibroblast images and SWCNT stability in media. See DOI: 10.1039/c2sm26995c

pro-inflammatory cytokine secretion.[28] However, there has been no quantitative evidence to determine how cellular activity is related to amount of SWCNT uptake.

An understanding of the mechanism of uptake is required both to gauge toxicity and to dose nanomaterials for cellular therapy. Traditionally, cellular uptake mechanisms are determined using either fluorescence labeling of cellular components or blocking cellular pathways with chemical agents. However, these methods are inapplicable with SWCNTs since nanotubes nonlinearly quench fluorescence,[29] which limits or eliminates the ability to precisely track materials within subcellular compartments. Also, the SWCNT–cell interaction is inherently non-specific and determining cellular uptake mechanisms using chemical blocking agents may lead to inconclusive results since chemical agents have broad, overlapping effects on cell processes.

Herein, we extract details of mechanistic uptake and underlying cellular effects by modulating SWCNT surface coating and quantifying associated variations in cellular activity. We employ Raman confocal imaging and spectroscopy to systematically measure nanotube uptake and subcellular localization as functions of nanotube surface coating with bioinert triblock copolymer, Pluronic F127, (PF127) and bioactive bovine serum albumin (BSA). We also quantify nanotube delivery with altered macrophage activity using LPS stimulation. Macrophages show a 100-fold increase in SWCNT uptake and adaptation of cellular size to accommodate SWCNTs, in contrast to fibroblasts. We combine these experimental measurements with models of passive and active cellular uptake[30,31] to estimate membrane *versus* receptor-mediated uptake of nanotubes into macrophages.

Materials and methods

SWCNT dispersion preparation

Unpurified SWCNTs (HiPCO (high-pressure carbon monoxide conversion synthesis), Carbon Nanotechnologies, Inc.) were purified according to previous methods, resulting in purified, unaltered SWCNTs (<5 wt% carbonaceous impurities, ~0.3 wt% metallic impurities).[32,33] As described previously, individual SWCNTs were isolated from bundles[34,35] and length fractionated using a density gradient,[36] resulting in SWCNTs with lengths[37] of 145 ± 17 nm and diameters of 1 ± 0.3 nm. For this work, purified and length fractionated SWCNTs were dispersed in ultrapure water using either Pluronic F127 (PF127; BASF) or bovine serum albumin (BSA; Sigma-Aldrich) at a SWCNT : PF127 or SWCNT : BSA ratio of 1 : 10 by weight for a final SWCNT concentration of 0.1 wt%. The solutions were probe-tip sonicated for 2 h at 60 W. Solutions were centrifuged (Beckman Coulter Allegra 25R Centrifuge with TA-15-1.5 rotor) at 21 000 × *g* for 30 min (SWCNTs–PF127) or 7 min (SWCNTs–BSA) to remove bundles. The supernatants were collected and examined using vis–NIR absorbance spectroscopy (Varian Cary 5000 Spectrophotometer), and concentrations were determined using an extinction coefficient of 2.6 (absorbance mL (mg mm)$^{-1}$) at 930 nm.[36] Characterization of PF127 and BSA dispersed SWCNTs has been examined in detail elsewhere.[24,25] Supernatants were sterilized by ultraviolet light for 1 h before use in cell experiments.

Cell culture and treatment

J774A.1 murine macrophage-like cells (ATCC, Catalog #TIB-67) were cultured in Dulbecco's Modified Eagle's Medium (high glucose (4500 mg L^{-1}), 4.0 mM L-glutamine and with no sodium pyruvate (Thermo Scientific Hyclone, Catalog #SH30022) supplemented with 10% v/v fetal bovine serum (Invitrogen) and 1% v/v penicillin–streptomycin (Invitrogen). NIH-3T3 murine fibroblast cells were cultured in similar media with newborn calf serum, not fetal bovine serum (Invitrogen).

J774A.1 cells were seeded at 2.0 × 10^4 cells per cm^2 or NIH-3T3 cells were seeded at 3.0 × 10^4 cells per cm^2 in 96-well plates and maintained for 24 h. SWCNTs–PF127 or SWCNTs–BSA were diluted to the indicated concentrations in fresh cell culture media and added to the cells. Ultrapure, sterile filtered water was diluted in cell culture media for sham experiments to ensure the same total volume and dilution for every well. Each treatment condition was performed in triplicate. As indicated cases with J774A.1 cells, lipopolysaccharide (LPS; Invitrogen, Catalog #L4391) was added with SWCNTs at a concentration of 5 μg mL^{-1}. Cells were maintained in culture for 48 h, after which the media was removed. Cells were then gently washed once with phosphate-buffered saline (PBS; Invitrogen).

To determine cells per well, 180 μL of PBS was added to each well, and the cells were quickly imaged using phase contrast on a Nikon Eclipse TS100 with a 20× (0.4 NA) dry objective (n > 5 fields of view with ~0.1 mm^2 per field). The total cell count per well was determined by manually counting cells per field of view and extrapolating the density to the entire well area. Projected cell area was measured by tracing cell outlines and quantified using ImageJ. For J774A.1 and NIH-3T3 cells, >250 and >80 cells, respectively, per condition were analyzed. Statistical analysis between indicated groups was performed with a Student's t-test of means.

Determination of proliferation and viability

J774A.1 cells were seeded at 5 × 10^3 cells per cm^2 in 6-well plates and maintained in culture for 24 h. As in other experiments, SWCNTs were diluted to the indicated concentrations in fresh cell culture media and added to the cells; 1 wt% PF127 or BSA solutions were also investigated for cellular effects. Cells with the indicated treatments were maintained in culture for 48 h. Subsequently, the media with SWCNTs was removed and replaced with fresh media (without phenol red) for imaging. Hoechst 33342, a cell permeable nucleic acid stain, and propidium iodide (PI), a cell impermeable nucleic acid stain, were added for quantification of total cells and dead cells, respectively. Images were taken (n > 10 fields of view with ~0.4 mm^2 per field) in phase contrast, blue fluorescence (Hoechst 33342) and red fluorescence (PI) on a Leica DMI 6000B inverted light and fluorescence microscope maintained at 37 °C with a 20× (0.4 NA) dry objective. For each condition, >10 fields of view with ~2000 cells were analyzed. Nuclei were automatically segmented and enumerated using ImageJ with manual

verification for accurate segmentation. Proliferation was measured as a percentage of cells normalized to control cell count. Viability was measured by PI exclusion normalized to total cell count with Hoechst.

Quantification of SWCNT uptake

After imaging, cells were incubated in lysis buffer (Cell Signaling Technologies) at 4 °C for 1 h and then exposed to probe tip sonication for 10 s at 60 W. To quantify the concentration of SWCNTs per well, the sonicated lysate solutions were pipetted into a 24-well glass (#1.5) bottom plate (MatTek) and subjected to Raman confocal imaging (inVia Raman microscope, Renishaw) with a 785 nm laser (100 mW) and a 50× (0.9 NA) dry objective. SWCNT concentration was determined from the intensity of the graphene band (G-band) at 1590 cm^{-1} using a standard curve previously reported by our group.[24] Precise measurements of G-band counts relative to the standard curve across multiple days were ensured by calibrating to the same silicon standard before each experiment. Uncertainties in our measurement of SWCNTs per cell reflect the propagation of uncertainties in measurements of total cell count per well and G-band counts. We calculated an approximate number of SWCNTs from the experimentally measured mass using the molecular weight of a single SWCNT. Briefly, the molecular weight was determined by considering the number of unit cell repeats along the average 1 nm diameter and an average length of 145 nm for our SWCNTs, using an sp^2 carbon–carbon bond length of 1.421 Å.

Model and parameter fitting

The receptor mediated model was fit to SWCNTs–BSA uptake data using a nonlinear least squares method available in the MATLAB Curve Fitting Toolbox software (MathWorks). Full derivation of the model and parameter fitting assumptions are available in ESI.†

Raman confocal imaging and spectroscopy

For imaging experiments, J774A.1 cells were seeded at 5.0×10^3 cells per cm^2 onto sterilized 22 × 22 mm glass coverslips (Fisher) placed in 35 mm cell culture dishes and maintained for 24 h. SWCNTs–PF127 and SWCNTs–BSA were diluted to 30 μg mL^{-1} in fresh cell culture media and added to the cells. After 48 h, the media containing SWCNTs was removed. Cells were then gently washed three times in PBS and subsequently fixed with 3.7% v/v formaldehyde (Sigma-Aldrich) for 15 min. Phase contrast imaging and Raman confocal imaging were performed on an inverted Raman confocal microscope (inVia Raman microscope, Renishaw) with a 785 nm laser (100 mW) and a 100× (1.4 NA) oil immersion objective. Static scans for 100 ms around the G-band (1327–1819 cm^{-1}) were collected with an acquisition step size of 1 μm over a concatenation of 9 fields of view. Spatial maps of the G-band signal intensity (1590 ± 15 cm^{-1}) above the baseline signal were performed in WiRE software (Renishaw).

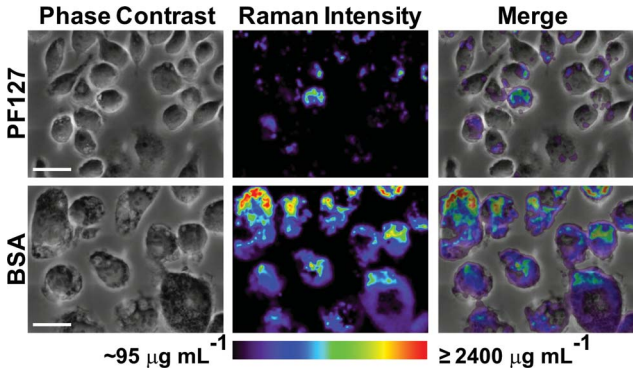

Fig. 1 High magnification images of SWCNT uptake in macrophages. Phase contrast images were co-registered to quantitative intracellular SWCNT signal (G-band, 1590 cm^{-1}) to generate spatial maps of SWCNT uptake. Cells treated with SWCNTs–PF127 exhibited small pockets of relatively low-level uptake. Cells treated with SWCNTs–BSA showed a homogeneous distribution of low-level uptake, as well as larger pockets of high-level uptake. In both cases, the majority of concentrated SWCNT pockets were located in the perinuclear space and regions along the cell periphery. The color scale bar is the approximate local concentration of SWCNTs in the range of 95–2400 μg mL^{-1}. (Scale bar = 20 μm.)

Results and discussion

Subcellular localization of SWCNTs inside macrophages

We investigated the subcellular localization of SWCNTs inside macrophages with high magnification phase contrast imaging superimposed with Raman confocal imaging and spectroscopy. We use Raman spectroscopy for imaging and quantification since the Raman G-band signal of SWCNTs is linear with concentrations over several orders of magnitude.[31] Cells exposed to SWCNTs–PF127 and SWCNTs–BSA at 30 μg mL^{-1} for 48 h were fixed and imaged under phase contrast and Raman microscopy. Raman intensity maps of the G-band signal (1590 cm^{-1})[38] were taken at the midline of the cell in the same field of view and co-registered to the phase contrast images to generate a quantitative spatial distribution of SWCNT concentration inside macrophages (Fig. 1). We observed a relatively homogeneous uptake of SWCNTs within the population of cells for each condition. Cells treated with SWCNTs–PF127 showed small pockets of concentrated subcellular localization. Cells treated with SWCNTs–BSA showed a homogeneous distribution of less concentrated uptake, but larger pockets of highly concentrated SWCNTs were also observed. With both types of surface coatings, the majority of concentrated SWCNT pockets were located in the perinuclear space and regions along the cell periphery, consistent with normal cell processing from phagocytosis and pinocytosis accumulation (Fig. 1 and S1†).

SWCNT dosage and surface coating alters macrophage morphology

Since macrophages internalized high levels of SWCNTs, possibly by compartmentalization, we examined gross changes in macrophage morphology. Bioinert SWCNTs–PF127 caused no observable changes in macrophage morphology, but bioactive SWCNTs–BSA dramatically altered cellular morphology with

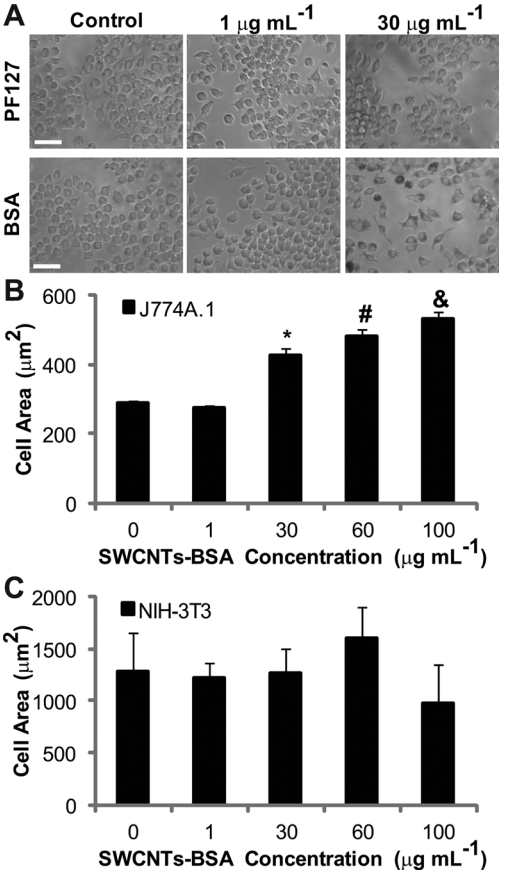

Fig. 2 SWCNT concentration- and coating-dependent effects on macrophage morphology. (A) Low magnification images show a dose-dependent change in morphology with noticeable phase dense regions for macrophages treated with SWCNTs–BSA but not SWCNTs–PF127. (Scale bar = 50 μm.) (B) Projected cell area for J774A.1 macrophages treated with SWCNTs–BSA increased with SWCNT concentration (mean ± standard deviation, 40 cells per FOV, 2 FOV per well, 3 wells; $^{*}p < 0.001$ compared to control, $^{\#}p < 0.05$ compared to 30 μg mL^{-1}, $^{\&}p < 0.05$ compared to 60 μg mL^{-1}). (C) Quantified cell area for NIH-3T3 fibroblasts was found to be independent of treatment with SWCNTs–BSA (mean ± standard deviation, 20 cells per FOV, 4 FOV per well, 1 well).

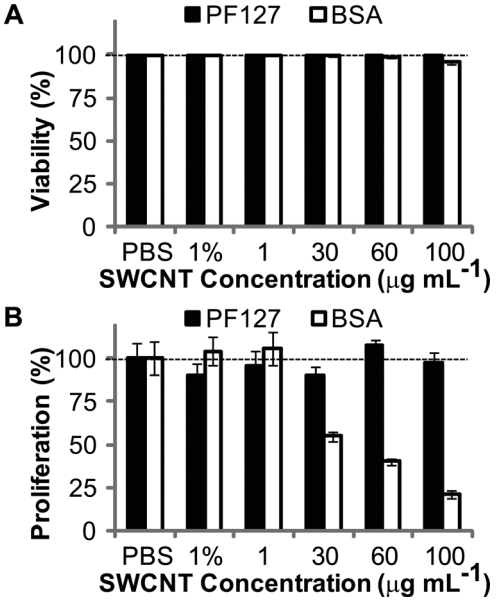

Fig. 3 Macrophage viability and proliferation with SWCNT concentration and coating. (A) No significant reduction in viability was observed for SWCNTs–PF127, while a minor, yet statistically significant, reduction (to 95%) was observed for SWCNTs–BSA at the highest concentration. Viability was measured as the percentage of propidium iodide (PI) negative cells. (B) Macrophage proliferation remained statistically unaltered for SWCNTs–PF127 but was statistically reduced in a dose-dependent manner for high concentrations of SWCNTs–BSA. Proliferation was measured by cell enumeration and represented relative to control. Data represent mean ± SEM, >50 cells per FOV, 10 FOV per well, 1 well.

increasing SWCNT concentration (Fig. 2A). At SWCNTs–BSA concentrations >30 μg mL^{-1}, we observed distinctly phase-dense cytoplasmic regions. To compare these morphological changes, we measured projected macrophage area with increasing amounts of SWCNTs–BSA. At SWCNTs–BSA concentrations >30 μg mL^{-1}, we observed statistically significant, dose-dependent increases in projected cell area (Fig. 2B). These phenotypic changes associated with SWCNTs–BSA were cell-type specific: fibroblasts exposed to the same range of SWCNT concentrations showed neither phase-dense cytoplasm (Fig. S2, ESI†) nor dramatic size differences with exposure to SWCNTs–BSA (Fig. 2C). Note that SWCNT uptake into epithelial and mesenchymal stem cells showed little change in cell morphology at SWCNTs–BSA concentrations up to 30 μg mL^{-1}.[22]

SWCNT dosage and surface coating affect macrophage proliferation

Since we aim to effectively deliver SWCNTs to macrophages, we examined how SWCNTs impact macrophage viability and proliferation in addition to cell morphology. Previously, we showed that SWCNTs are not acutely toxic but significantly reduce cell proliferation.[17] Similar to morphology, we found that cell viability and proliferation were not significantly impacted at any concentration for SWCNTs–PF127 (Fig. 3). SWCNTs–BSA statistically reduced macrophage viability, but >95% of cells remained viable even at extremely high SWCNT concentrations (Fig. 3A). Despite minimal effects on cell survival, SWCNTs–BSA dramatically reduced cell proliferation in a dose-dependent way at concentrations >30 μg mL^{-1} (Fig. 3B). The reduction in proliferation also corresponded to the increase in cell size observed for SWCNTs–BSA >30 μg mL^{-1} (Fig. 2B). However, macrophages treated with 30 μg mL^{-1} of SWCNTs–BSA showed a much different physical morphology (Fig. 2) and altered viability and proliferation (Fig. 3) compared with an equivalent (100 μg mL^{-1} treatment) number of internalized SWCNTs–PF127. Macrophages may be comparatively more sensitive to bioactive SWCNTs–BSA than SWCNTs–PF127 not only because of the greater internalized SWCNT concentration but perhaps also due to the preferential receptor based uptake and subsequent cellular processing.

Modeling of receptor- and membrane-mediated uptake *via* modulation of SWCNT surface coating

We quantified SWCNT concentration inside cells using a calibration curve that relates G-band intensity of the Raman spectra at 1590 cm^{-1} to SWCNT concentration.[24] We treated cells with SWCNTs for 48 h, washed with phosphate buffered saline (PBS),

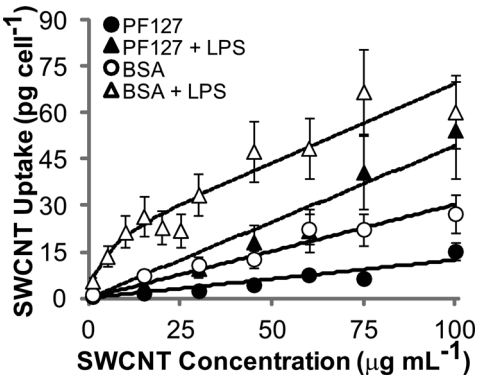

Fig. 4 Quantified uptake per cell for macrophages with different SWCNT surface coatings and cellular activity levels. SWCNTs–BSA showed enhanced uptake per cell compared to SWCNTs–PF127. For indicated points, cells were prestimulated with 5 μg mL^{-1} lipopolysaccharide (LPS), which further increased uptake. Treatment of LPS stimulated macrophages with SWCNTs–BSA shows saturated uptake. Lines represent the best linear or nonlinear fits to the data (see Methods). Data represent mean ± SEM obtained through error propagation, ≥3 FOV per well, 3 wells.

lysed the cells and measured internalized and membrane-associated SWCNTs using Raman spectroscopy of the lysates. Cells treated with SWCNTs–PF127 showed increased uptake with increased exposure concentration, from 0.1 pg per cell at 1 μg mL^{-1} SWCNT to 15 pg per cell at 100 μg mL^{-1} SWCNT (Fig. 4). Pluronics are membrane active and we have previously reported that Pluronic F127 coating increases the association of SWCNTs with cell membranes and other cell structures.[39,40] We attribute SWCNTs–PF127 internalization to association with the cell surface and express SWCNT internalization *via* membrane uptake with first order kinetics.

$$[\mathrm{SWCNT}]_{\mathrm{int}} = K_{\mathrm{mem}}[\mathrm{SWCNT}]_{\mathrm{ext}} \quad (1)$$

$[\mathrm{SWCNT}]_{\mathrm{int}}$ and $[\mathrm{SWCNT}]_{\mathrm{ext}}$ are the internal and external concentration of SWCNTs, respectively, and K_{mem} has units of (pg per cell)/(μg mL^{-1} SWCNT). K_{mem} represents a superposition of steps including diffusion, membrane association, cell endocyosis and other cellular processes (see ESI†). From data of $[\mathrm{SWCNT}]_{\mathrm{int}}$ *versus* $[\mathrm{SWCNT}]_{\mathrm{ext}}$ in Fig. 4 and eqn (1), we determine K_{mem} to be 0.1 (pg per cell)/(μg mL^{-1} SWCNT).

SWCNTs–BSA showed increased cellular uptake with a maximum uptake of 27 pg per cell at 100 μg mL^{-1} (Fig. 4). Macrophages have surface receptors designed to bind numerous proteins[41] and show affinity for albumins and albumin-coated nanomaterials.[42] We hypothesize that the protein coating on SWCNTs enhanced uptake through stimulation or interaction with cell surface receptors leading to accelerated internalization. Thus, uptake is a function of K_{mem} from above as well as a receptor mediated effect K_{rec}.

$$[\mathrm{SWCNT}]_{\mathrm{int}} = (K_{\mathrm{mem}} + K_{\mathrm{rec}})[\mathrm{SWCNT}]_{\mathrm{ext}} \quad (2)$$

K_{rec} is dependent on receptor concentration. A reasonable form for K_{rec} can be taken as $K_{\mathrm{rec}} = K^0_{\mathrm{rec}}[R]$, but K^0_{rec} and receptor concentration, $[R]$, cannot be decoupled experimentally. From the data in Fig. 4 and eqn (2), we determine $(K_{\mathrm{mem}} + K_{\mathrm{rec}})$ to be 0.3 (pg per cell)/(μg mL^{-1} SWCNT), and $K_{\mathrm{rec}} = 0.2$ (pg per cell)/(μg mL^{-1} SWCNT). The receptor mediated uptake is double the uptake from nonspecific membrane association.

Modeling of receptor- and membrane-mediated uptake *via* modulation of macrophage activity

Specific targeting of SWCNTs to activated M1 macrophages has many potential uses including treatment of cancer, sensing and ablation of regions of chronic inflammation. To determine what role cell activity plays in SWCNT uptake, we stimulated macrophages with LPS, an endotoxin that specifically activates macrophages.[43] LPS induces activation of macrophages to an M1 phenotype[1] and increases pinocytosis and phagocytosis.[44,45] Macrophages were pre-stimulated with 5 μg mL^{-1} and treated with either SWCNTs–PF127 or SWCNTs–BSA.

With the bioinert SWCNTs–PF127, we observed a 4-fold increase in uptake, leading to a maximum uptake of 55 pg per cell at 100 μg mL^{-1} (Fig. 4). We attribute this increased uptake to increased pinocytosis and membrane processing, K'_{mem}.

$$[\mathrm{SWCNT}]_{\mathrm{int}} = K'_{\mathrm{mem}}[\mathrm{SWCNT}]_{\mathrm{ext}} \quad (3)$$

We found the experimental relation of external and internal concentration to be mostly linear, and $K'_{\mathrm{mem}} = 0.5$ (pg per cell)/(μg mL^{-1} SWCNT). Comparing uptake of SWCNTs–PF127 (K_{mem} *versus* K'_{mem}), we observed a 5-fold increase in membrane uptake with LPS stimulation. This 5-fold increase in membrane processing is consistent with previous reports of macrophage pinocytosis of small molecules such as with stimulating conditions.[44] Thus, SWCNTs–PF127 provides a good approximation of membrane-mediated uptake.

LPS-enhanced uptake of bioactive SWCNTs–BSA exhibited a significantly different trend compared to previous experiments without cell stimulation. Uptake of SWCNTs–BSA by activated macrophages was impacted by both BSA bioactivity and cell activation state at low concentrations (<30 μg mL^{-1}) showing a 7-fold increase over SWCNTs–BSA in non-stimulated cells. However, at a dosage level >30 μg mL^{-1}, uptake increased linearly with dosage with a similar rate to that of SWCNTs–PF127. With high levels of SWCNTs–BSA we observed a non-linear response (Fig. 4). Previously, immune cell uptake of acetylated low density lipoprotein[46] and starch particles[47] also demonstrated saturation at high exposure concentrations. This change in functional form of uptake could arise from receptor saturation. We modeled the receptor mediated portion of SWNCTs–BSA uptake with a saturation model.

$$[\mathrm{SWCNT}]_{\mathrm{int}} = K'_{\mathrm{mem}}[\mathrm{SWCNT}]_{\mathrm{ext}} + \frac{\alpha[\mathrm{SWCNT}]_{\mathrm{ext}}}{\beta + [\mathrm{SWCNT}]_{\mathrm{ext}}} \quad (4)$$

The parameters α and β reflect receptor saturation (see ESI†). When $[\mathrm{SWCNT}]_{\mathrm{ext}}$ is low, compared with levels of receptors, the $[\mathrm{SWCNT}]_{\mathrm{int}}$ eqn (4) becomes eqn (5) (see ESI†).

$$[\mathrm{SWCNT}]_{\mathrm{int}} = (K'_{\mathrm{mem}} + K'_{\mathrm{rec}})[\mathrm{SWCNT}]_{\mathrm{ext}} \quad (5)$$

Below 30 μg mL^{-1}, we determined that $(K'_{\mathrm{mem}} + K'_{\mathrm{rec}}) = 2.0$ (pg per cell)/(μg mL^{-1} SWCNT). From $K'_{\mathrm{mem}} =$ (pg per cell)/(μg mL^{-1} SWCNT), we approximate $K'_{\mathrm{rec}} = 1.5$ (pg per cell)/(μg mL^{-1}

SWCNT). Thus, in the limiting case of low SWCNT exposure concentration, the receptor mediated processes contribute three times as much as membrane mediated processes to overall macrophage uptake of SWCNTs, before losing effectiveness at high SWCNT exposure concentration as receptors begin to saturate. Providing these comparable quantitative parameters of cell uptake is not possible with traditional methods, such as chemical blocking of cellular processes (*e.g.*, endocytosis blocking with dynamin inhibitors). Since (i) the equilibrium coefficients are less than an order of magnitude different from one another, and (ii) SWCNTs enter cells by both non-specific membrane turnover and receptor-mediated processes, it would have been nearly impossible to decouple the quantitative effects of both with blocking.

We found that protein-coated SWCNTs entered cells using both non-specific and receptor-mediated processes; ~25 pg per cell SWCNTs–BSA was delivered to activated macrophages with as little as 10 μg mL^{-1} extracellular concentration. When considering SWCNT size (~145 nm long), this mass correlates to more than 50 million SWCNTs per cell.[22] This same level of delivery would require ≥100 μg mL^{-1} SWCNTs–BSA in non-stimulated macrophages. This suggests that SWCNTs can be preferentially delivered to activated macrophages (10 : 1) at 10 μg mL^{-1}. Further, the apparent saturation of receptor-mediated uptake over 30 μg mL^{-1} suggests that additional SWCNTs–BSA would have little added benefit. Previous studies of SWCNT delivery to macrophages examined conditions of 5–20 μg mL^{-1},[8,18,26] which was below the receptor threshold that we have observed.

Comparison of SWCNT uptake in fibroblasts *versus* macrophages

We are able to show an optimal SWCNT concentration for targeting activated macrophages. Another common cell type found in niches associated with macrophages – in wound healing, inflammation and repair – is a fibroblast. Therefore, we examined SWCNT uptake by fibroblasts using similar conditions to macrophages. The results followed the same trend observed for SWCNT uptake in macrophages; SWCNTs–BSA increased uptake 5-fold compared to SWCNTs–PF127 with maximum uptake of 3 and 14 pg per cell for SWCNTs–PF127 and SWCNTs–BSA, respectively (Fig. 5). Generally, macrophage uptake was 5–10 times greater than fibroblast uptake for comparable SWCNT dispersions. Since fibroblasts have intrinsically different sizes than macrophages, and macrophage size varies with SWCNT uptake, we considered the SWCNT uptake data with respect to projected cell area. The uptake of SWCNTs–BSA per unit area for macrophages showed a stronger concentration dependence than SWCNTs–BSA uptake for fibroblasts (~6 times greater). Taken together with the intracellular Raman maps (Fig. 1), macrophages appear to concentrate SWCNTs–BSA within their intracellular space compared to fibroblasts. As macrophages increase their uptake per cell, not only do they become larger in size, but the larger macrophages are packed more densely with SWCNTs.

In comparison to other published results of SWCNT uptake by macrophage cell lines, we observe 2–40 fold higher uptake. While no direct comparison exists, RAW 264.7 macrophages showed slightly reduced uptake (~2 fold less) of lipid-functionalized SWCNTs than observed here.[18] Extremely long, dispersed SWCNTs (10× longer than the ones studied here) show a 40-fold reduced uptake by J774A.1.[8] However, most studies do agree that professional phagosomes have increased nanoparticle uptake over other cells.

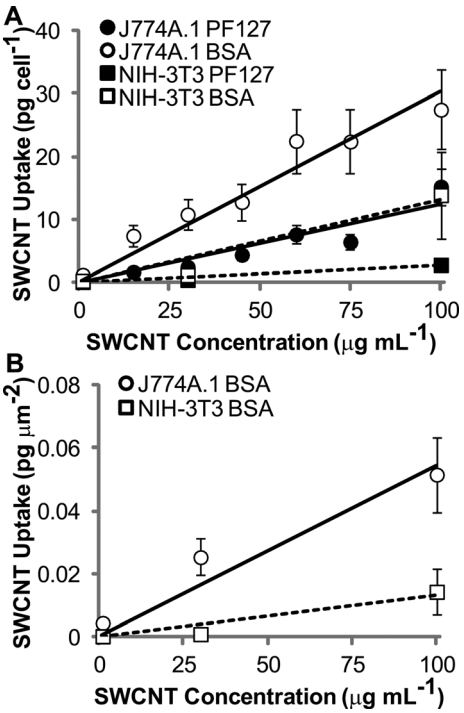

Fig. 5 Differential surface coating mediated SWCNT uptake in J774A.1 macrophages and NIH-3T3 fibroblasts. (A) Similar to macrophages, SWCNTs–BSA showed enhanced uptake per cell compared to SWCNTs–PF127 in fibroblasts. For comparable surface coatings, macrophages showed increased uptake trends compared to fibroblasts for both PF127 and BSA coatings. (B) Concentration-dependent uptake of SWCNTs–BSA per projected cell area was enhanced for macrophages, which is more than double the enhancement observed on a per cell basis. Data represent mean ± SEM obtained through error propagation, ≥3 FOV per well, 3 wells.

Conclusions

Bioactivity of the SWCNT coating and macrophage activity are both important for SWCNT uptake, but macrophage activity contributed more to levels of uptake. Even non-activated macrophages were able to internalize an order of magnitude more SWCNTs–BSA than fibroblasts, possibly by cell adaptation to engulfed materials. However, treatment concentrations >30 μg mL^{-1} are limited, likely since cell surface receptors were saturated. At these high levels, macrophages also showed altered morphology and proliferation. Thus we suggest a high potential for selective delivery of SWCNTs to M1 activated macrophages for imaging, sensing, drug delivery and ablation.

Acknowledgements

This work was supported by the NSF (CBET-0708418 and DMR-0619424 (K.N.D. and M.F.I.), DMR-0645596 (M.F.I.)), the Sloan Foundation (M.F.I.) and DOD (NDSEG) 32-CFR-168a (B.D.H.).

Notes and references

1 A. Mantovani, A. Sica, S. Sozzani, P. Allavena, A. Vecchi and M. Locati, *Trends Immunol.*, 2004, **25**, 677–686.
2 W. Ulbrich and A. Lamprecht, *J. R. Soc., Interface*, 2010, **7**, S55–S66.
3 F. Chellat, Y. Merhi, A. Moreau and L. H. Yahia, *Biomaterials*, 2005, **26**, 7260–7275.
4 D. M. Mosser and J. P. Edwards, *Nat. Rev. Immunol.*, 2008, **8**, 958–969.
5 N. W. S. Kam, M. O'Connell, J. A. Wisdom and H. Dai, *Proc. Natl. Acad. Sci. U. S. A.*, 2005, **102**, 11600–11605.
6 S. Madsen, S.-K. Baek, A. Makkouk, T. Krasieva and H. Hirschberg, *Ann. Biomed. Eng.*, 2012, **40**, 507–515.
7 A. Bianco, K. Kostarelos and M. Prato, *Curr. Opin. Chem. Biol.*, 2005, **9**, 674–679.
8 P. Cherukuri, S. M. Bachilo, S. H. Litovsky and R. B. Weisman, *J. Am. Chem. Soc.*, 2004, **126**, 15638–15639.
9 D. A. Heller, S. Baik, T. E. Eurell and M. S. Strano, *Adv. Mater.*, 2005, **17**, 2793–2799.
10 H. Jin, D. A. Heller and M. S. Strano, *Nano Lett.*, 2008, **8**, 1577–1585.
11 H. Jin, D. A. Heller, R. Sharma and M. S. Strano, *ACS Nano*, 2009, **3**, 149–158.
12 N. F. Reuel, A. Dupont, O. Thouvenin, D. C. Lamb and M. S. Strano, *ACS Nano*, 2012, **6**, 5420–5428.
13 I. Heller, W. T. T. Smaal, S. G. Lemay and C. Dekker, *Small*, 2009, **5**, 2528–2532.
14 J.-H. Kim, D. A. Heller, H. Jin, P. W. Barone, C. Song, J. Zhang, L. J. Trudel, G. N. Wogan, S. R. Tannenbaum and M. S. Strano, *Nat. Chem.*, 2009, **1**, 473–481.
15 M. J. O'Connell, S. M. Bachilo, C. B. Huffman, V. C. Moore, M. S. Strano, E. H. Haroz, K. L. Rialon, P. J. Boul, W. H. Noon, C. Kittrell, J. Ma, R. H. Hauge, R. B. Weisman and R. E. Smalley, *Science*, 2002, **297**, 593–596.
16 J.-P. Kaiser, P. Wick, P. Manser, P. Spohn and A. Bruinink, *J. Mater. Sci.: Mater. Med.*, 2008, **19**, 1523–1527.
17 B. D. Holt, P. A. Short, A. D. Rape, Y.-l. Wang, M. F. Islam and K. N. Dahl, *ACS Nano*, 2010, **4**, 4872–4878.
18 N. V. Konduru, Y. Y. Tyurina, W. Feng, L. V. Basova, N. A. Belikova, H. Bayir, K. Clark, M. Rubin, D. Stolz, H. Vallhov, A. Scheynius, E. Witasp, B. Fadeel, P. D. Kichambare, A. Star, E. R. Kisin, A. R. Murray, A. A. Shvedova and V. E. Kagan, *PLoS One*, 2009, **4**, e4398.
19 M. Zheng, A. Jagota, E. D. Semke, B. A. Diner, R. S. McLean, S. R. Lustig, R. E. Richardson and N. G. Tassi, *Nat. Mater.*, 2003, **2**, 338–342.
20 D. A. Tsyboulski, E. L. Bakota, L. S. Witus, J.-D. R. Rocha, J. D. Hartgerink and R. B. Weisman, *J. Am. Chem. Soc.*, 2008, **130**, 17134–17140.
21 D. Nepal and K. E. Geckeler, *Small*, 2007, **3**, 1259–1265.
22 B. D. Holt, K. N. Dahl and M. F. Islam, *Small*, 2011, **7**, 2348–2355.
23 C. Ge, J. Du, L. Zhao, L. Wang, Y. Liu, D. Li, Y. Yang, R. Zhou, Y. Zhao, Z. Chai and C. Chen, *Proc. Natl. Acad. Sci. U. S. A.*, 2011, **108**, 16968–16973.
24 B. D. Holt, K. N. Dahl and M. F. Islam, *ACS Nano*, 2012, **6**, 3481–3490.
25 B. D. Holt, M. C. McCorry, P. D. Boyer, K. N. Dahl and M. F. Islam, *Nanoscale*, 2012, DOI: 10.1039/c2nr31928d.
26 T. dos Santos, J. Varela, I. Lynch, A. Salvati and K. A. Dawson, *Small*, 2011, **7**, 3341–3349.
27 D. Dutta, S. K. Sundaram, J. G. Teeguarden, B. J. Riley, L. S. Fifield, J. M. Jacobs, S. R. Addleman, G. A. Kaysen, B. M. Moudgil and T. J. Weber, *Toxicol. Sci.*, 2007, **100**, 303–315.
28 H. Dumortier, S. Lacotte, G. Pastorin, R. Marega, W. Wu, D. Bonifazi, J.-P. Briand, M. Prato, S. Muller and A. Bianco, *Nano Lett.*, 2006, **6**, 1522–1528.
29 J. M. Wörle-Knirsch, K. Pulskamp and H. F. Krug, *Nano Lett.*, 2006, **6**, 1261–1268.
30 M. R. Birtwistle and B. N. Kholodenko, *Mol. Oncol.*, 2009, **3**, 308–320.
31 D. A. Lauffenburger and J. J. Linderman, *Receptors: Models for Binding, Trafficking, and Signaling*, Oxford University Press, New York, 1993.
32 D. E. Johnston, M. F. Islam, A. G. Yodh and A. T. Johnson, *Nat. Mater.*, 2005, **4**, 589–592.
33 M. F. Islam, D. E. Milkie, O. N. Torrens, A. G. Yodh and J. M. Kikkawa, *Phys. Rev. B: Condens. Mater. Phys.*, 2005, **71**, 201401(R).
34 M. F. Islam, E. Rojas, D. M. Bergey, A. T. Johnson and A. G. Yodh, *Nano Lett.*, 2003, **3**, 269–273.
35 M. S. Arnold, A. A. Green, J. F. Hulvat, S. I. Stupp and M. C. Hersam, *Nat. Nanotechnol.*, 2006, **1**, 60–65.
36 J. A. Fagan, M. L. Becker, J. Chun and E. K. Hobbie, *Adv. Mater.*, 2008, **20**, 1609–1613.
37 M. L. Becker, J. A. Fagan, N. D. Gallant, B. J. Bauer, V. Bajpai, E. K. Hobbie, S. H. Lacerda, K. B. Migler and J. P. Jakupciak, *Adv. Mater.*, 2007, **19**, 939–945.
38 M. S. Dresselhaus, G. Dresselhaus, R. Saito and A. Jorio, *Phys. Rep.*, 2005, **409**, 47–99.
39 P. N. Yaron, B. D. Holt, P. A. Short, M. Losche, M. F. Islam and K. N. Dahl, *J. Nanobiotechnol.*, 2011, **9**, 45.
40 B. D. Holt, H. Shams, T. A. Horst, S. Basu, A. D. Rape, Y. L. Wang, G. K. Rohde, M. R. K. Mofrad, M. F. Islam and K. N. Dahl, *J. Funct. Biomater.*, 2012, **3**, 398–417.
41 A. Aderem and D. M. Underhill, *Annu. Rev. Immunol.*, 1999, **17**, 593–623.
42 C. D. Walkey and W. C. W. Chan, *Chem. Soc. Rev.*, 2012, **41**, 2780–2799.
43 C. R. H. Raetz and C. Whitfield, *Annu. Rev. Biochem.*, 2002, **71**, 635–700.
44 P. J. Edelson, R. Zwiebel and Z. A. Cohn, *J. Exp. Med.*, 1975, **142**, 1150–1164.
45 M. L. Karnovsky, J. Lazdins, D. Drath and A. Harper, *Ann. N. Y. Acad. Sci.*, 1975, **256**, 266–274.
46 C. Buono, J. J. Anzinger, M. Amar and H. S. Kruth, *J. Clin. Invest.*, 2009, **119**, 1373–1381.
47 R. H. Michell, S. J. Pancake, J. Noseworthy and M. L. Karnovsky, *J. Cell Biol.*, 1969, **40**, 216–224.

